

Fast Switching Phase Calibration: Effectiveness at Mauna Kea and Chajnantor

M.A. Holdaway, Simon J.E. Radford, F.N. Owen, and Scott M. Foster
National Radio Astronomy Observatory

September 26, 1995

Abstract

We present estimates of how well fast switching phase calibration would perform at the Chajnantor, Chile, and Mauna Kea VLBA sites. Fast switching at Chajnantor would achieve better than 30° r.m.s. phase errors at 230 GHz about twice as often as at Mauna Kea. We also investigate how the residual phase errors depend upon the slew speed of the antennas (0.5° s^{-1} through 2.0° s^{-1}). At 230 GHz, faster slewing provides a significant improvement in the fraction of time the array will be able to achieve 30° r.m.s. residual phase errors. At 690 GHz, faster slewing will provide two or three times more observing time available with 30° r.m.s. residual phase errors. Increasing the total continuum bandwidth from 4 GHz to 16 GHz provides a marginal improvement in the residual phase errors.

1 Introduction

The primary goal of site testing is to compare site characteristics, such as opacity and phase stability, that will influence astronomical observing. A secondary goal is to predict with some confidence how well various observing strategies, such as fast switching phase calibration, will work. The data analysis for the site test interferometer was outlined in MMA Memo 129 (Holdaway, Radford, Owen, and Foster 1995), and residual phase errors after fast switching were analyzed in MMA Memo 126 (Holdaway and Owen 1995). Here we use the most current estimates of the distributions of the phase structure function and velocity aloft at Chajnantor, Chile, and at the Mauna Kea VLBA site to provide a better picture of how well fast switching will work at these sites.

2 Changes Since the Previous Fast Switching Analysis

The analysis of the fast switching phase calibration performed here is identical to the analysis described in MMA Memo 126, but we have changed a number of the input parameters in this work. The differences between the previous work and this work are summarized below:

- The current work uses distributions of the phase structure function and the velocity aloft measured with the NRAO site test interferometers. The Mauna Kea data were obtained between December 1994 and July 1995, while the Chajnantor data were obtained between May 6, 1995, and August 11, 1995. *Note the data cover the season when we expect the best conditions at Chajnantor, so the overall distribution of the phase structure function may degrade in the coming months.*
- The median velocity aloft at both sites is very close to 12.5 m s^{-1} , whereas the previous analysis used a velocity of 5 m s^{-1} determined by Colin Masson for the summit of Mauna Kea. We have used the data reduction path described in MMA Memo 129 (Holdaway, Radford, Owen, and Foster, 1995) to compare the site test data for the Mauna Kea summit and the Mauna Kea VLBA site. We found the median velocity aloft for the summit was about 6 m s^{-1} , in agreement with Masson’s result, but the median velocity at the lower altitude VLBA site was 12 m s^{-1} . This apparent contradiction is understood if the summit is dominated by surface turbulence that moves across the interferometer at close to the surface velocity while the VLBA site is dominated by turbulence at a much higher elevation. Larger velocities aloft result in larger residual phase errors with fast switching.
- The median power law index of the phase structure function is 0.61 at Chajnantor and 0.62 at the Mauna Kea VLBA site.
- We fixed a bug in the code that determined the optimal value of $vt/2+d$ for each simulated calibrator field, resulting in somewhat larger residual phase errors in most cases.
- We performed calculations for total continuum bandwidths of 4 GHz and 16 GHz, the two possibilities currently under discussion.
- We considered a range of slewing speeds and setup times: 0.5° s^{-1} and 2 s setup, 1° s^{-1} and 1 s setup, and 2° s^{-1} and 0.5 s setup. Currently the antenna group is confident switching to a source 1.5° away can be accomplished in about 2 s, roughly equivalent to 1° s^{-1} and 1 s setup.
- Most simulations were performed with $2/3$ of the cycle time integrating on the target source, which increases the noise by 22% over spending all the time on source. One set of simulations explored how the residual phase errors depend upon the fraction of time spent on source while fixing the time on the calibrator.
- Sources as weak as 10 mJy were included in the Monte Carlo simulation of the calibrator distribution.

Our site test database includes a time series of the phase structure function amplitude, its power law exponent, and the velocity aloft. Eventually we hope to use all of this information since these quantities are not independent. For now, however, we have used the full distribution of the structure function amplitude and the median velocity and power law exponent.

3 Cumulative Distributions of Residual Phase Errors for Fast Switching

The residual phase errors after fast switching phase calibration are

$$\sigma_\phi = \sqrt{D_\phi(vt/2 + d)} \quad (1)$$

(MMA Memo 126), and are independent of baseline length for baselines longer than $vt/2 + d$. Note that fast switching phase calibration will work for arbitrarily long baselines. The residual phase errors can be calculated for any simulated calibrator/source configuration, observing strategy, and instrument sensitivity. Given the distribution of the structure function, D_ϕ , we can create a distribution of residual phase errors that includes both the distribution of calibrators on the sky and the distribution of atmospheric conditions. We assume acceptable images can be made with 30° r.m.s. errors.

Figure 1 shows the distributions of residual phase errors after fast switching calibration at Chajnantor with 16 GHz of continuum bandwidth, corrected for 60 degrees elevation angle, calculated for a range of simulated switching speeds. The measured distribution of atmospheric phase fluctuations on a 300 m baseline and the extrapolated distribution of phase fluctuations on a 1000 m baseline are also shown. Figure 2 shows the same distributions for Chajnantor with a 4 GHz continuum bandwidth and figures 3 and 4 show the analogous data for the Mauna Kea VLBA site. Figure 5 shows the residual phase error distributions for the Chajnantor and Mauna Kea sites together. Figure 6 shows the residual phase errors improve when a smaller fraction of the cycle time is spent on the target source, making the entire cycle faster since the integration time on the calibrator is fixed.

4 Conclusions

- **The 16 GHz bandwidth** improves fast switching only moderately. Because the sensitivity, the typical distance to the nearest detectable calibrator, and the phase structure function all depend sub-linearly on the bandwidth, increasing the bandwidth by a factor of 10 will decrease the residual phase errors by only a factor of about 1.5. The extra bandwidth will help most with the very small phase error case (i.e., high frequencies).
- **Switching speed** is moderately important for 230 GHz and crucial for higher frequencies. Improving the switching time for a 1° move from 4 s (0.5° s^{-1} and 2 s setup) to 2 s (1° s^{-1} and 1 s setup) would improve the residual phase errors at 230 GHz at Chajnantor by about 10° , making the array usable about 10% more often. Observations at 690 GHz would require 10° r.m.s. phase errors on our 230 GHz plots. At 690 GHz, the same improvement would double the amount of time available for observations.
- **Fraction of time on the target source.** The residual phase errors can be reduced, to some limit, by spending a smaller fraction of each cycle on the target source. We fixed

the time on the calibrator, so this speeds up the entire cycle. Figure 6 shows this effect for Chajnantor, 1° s^{-1} switching, and 16 GHz bandwidth. If 30° r.m.s. phase errors are acceptable, spending 83% of the cycle time on the target source (increasing the noise by 10%) will work just over half the time. If the atmospheric conditions are marginal, reducing the source integration to 50% of the cycle time (41% noise increase) will permit observations with 30° r.m.s. phase errors 75% of the time. After this, returns diminish quickly, since the cycle time, and hence $vt/2 + d$, will be limited by the slew time, the distance between source and calibrator, and the detection time for the calibrator.

- **Chajnantor and Mauna Kea.** In comparing these sites, we must bear in mind our data from Chajnantor only cover three months and we expect these are the best months of the year. Nevertheless, the data we have now indicate high frequency, long baseline observations would be possible only about half as often at the Mauna Kea VLBA site as at Chajnantor.

References

- Holdaway, M.A., and Ishiguro, Masato, 1995, MMA Memo 127, “Dependence of Tropospheric Path Length Fluctuations on Airmass.”
- Holdaway, M.A., and Owen, F.N., 1995, MMA Memo 126, “A Test of Fast Switching Phase Calibration with the VLA at 22 GHz.”
- Holdaway, M.A., Ishiguro, Masato, and Morita, K.-I., 1995, MMA Memo ???, “Analysis of the Spatial and Temporal Phase Fluctuations Above Nobeyama.”
- Holdaway, M.A., Radford, Simon J.E., Owen, F.N., and Foster, Scott M., 1995, MMA Memo 129, “Data Processing for Site Test Interferometers.”
- Holdaway, M.A., Radford, Simon J.E., Masson, C., Owen, F.N., and Foster, Scott M., 1995, MMA Memo ???, “Phase Stability Comparison of the VLBA and Millimeter Valley Mauna Kea Sites.”

Chile Residual Phase Error @ 230 GHz, V=12m/s, 16 GHz BW

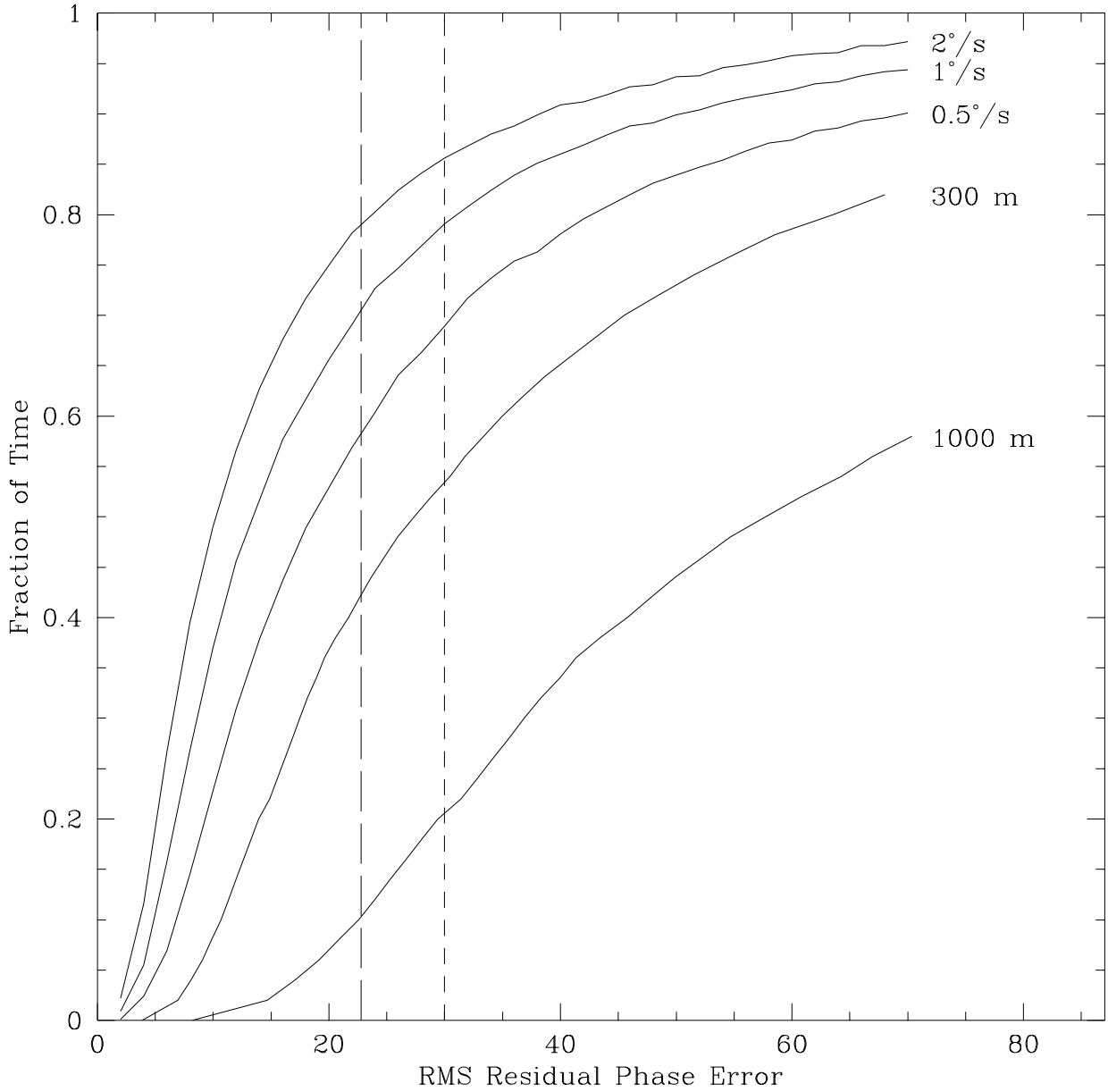


Figure 1: Cumulative distributions of residual phase errors at 60 degree elevation after fast switching with 16 GHz bandwidth at Chajnantor for three different switching speeds. Distributions of uncorrected atmospheric phase fluctuations on 300 m and 1000 m baselines are show for comparison. The two dashed vertical lines represent the 30 degree rms phase limit required at elevation angle of 60 degrees, and 23 degrees rms phase, which translates to 30 degrees rms phase at an elevation angle of 30 degrees.

Chile Residual Phase Error @ 230 GHz, $V=12\text{m/s}$, 4 GHz BW

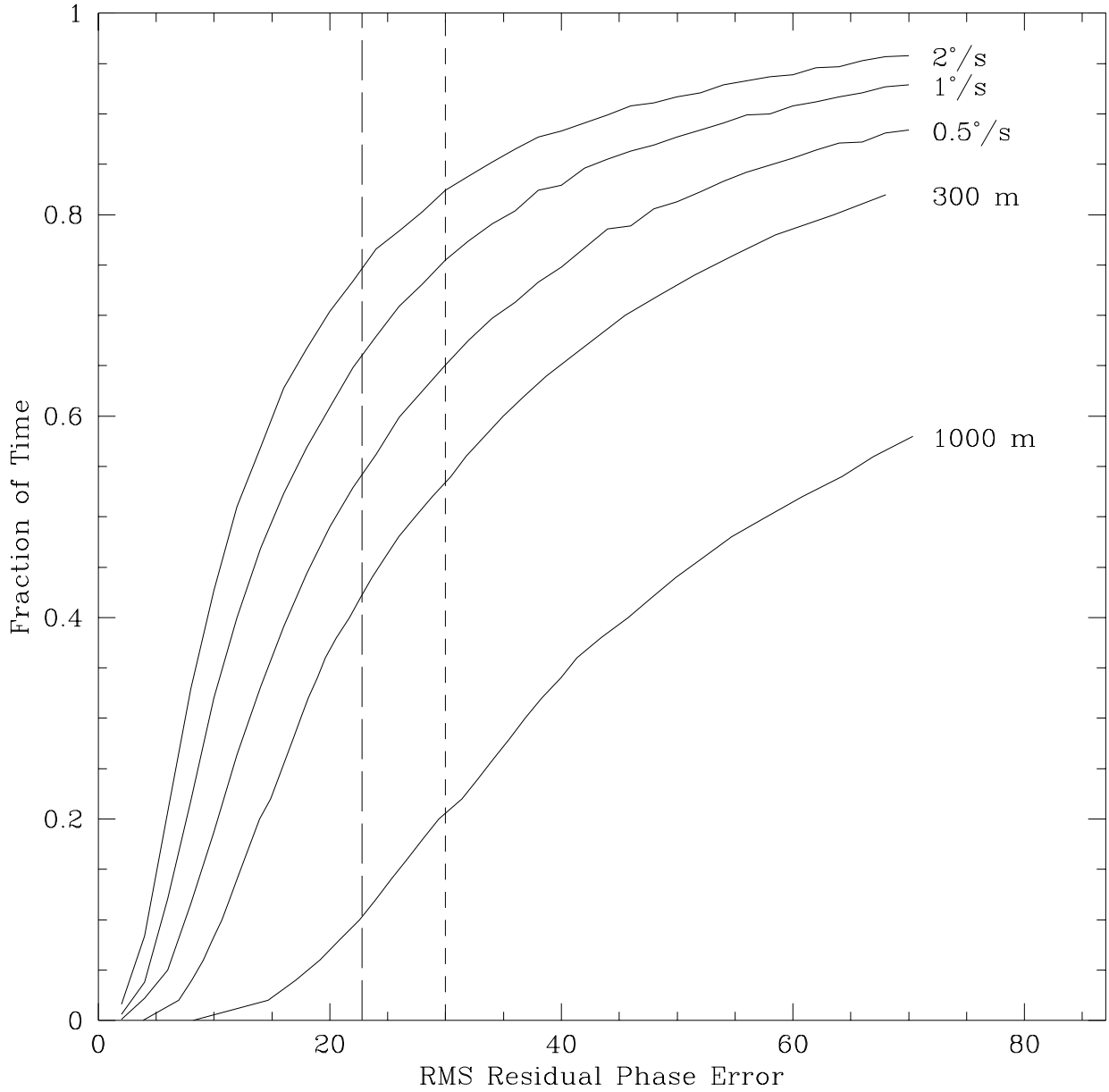


Figure 2: Cumulative distributions of residual phase errors after fast switching with 4 GHz bandwidth at Chajnantor for three different switching speeds. Distributions of uncorrected atmospheric phase fluctuations on 300 m and 1000 m baselines are show for comparison.

MK Residual Phase Error @ 230 GHz, V=12m/s, 16 GHz BW

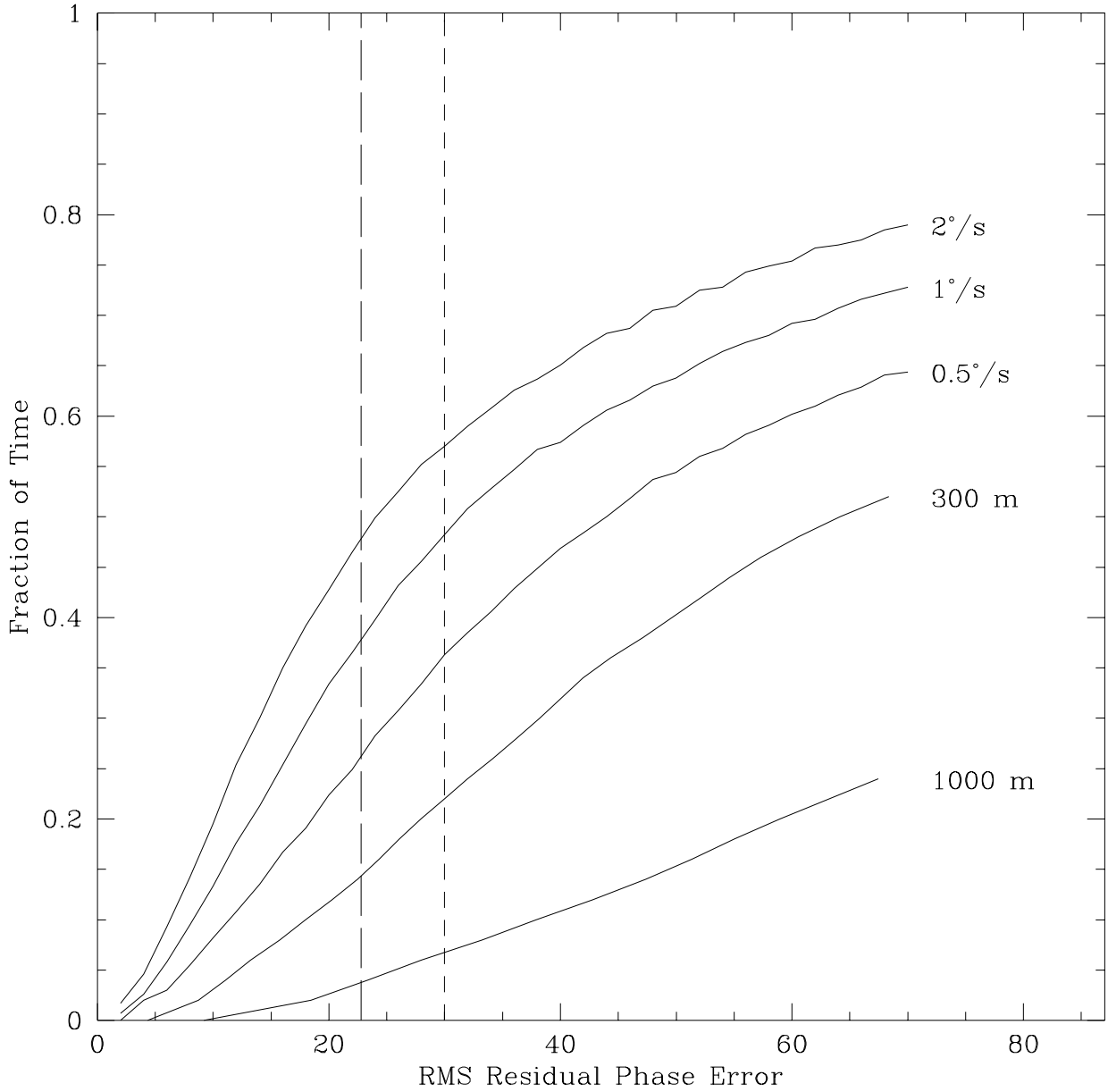


Figure 3: Cumulative distributions of residual phase errors after fast switching with 16 GHz bandwidth at the Mauna Kea VLBA site for three different switching speeds. Distributions of uncorrected atmospheric phase fluctuations on 300 m and 1000 m baselines are show for comparison.

MK Residual Phase Error @ 230 GHz, $V=12\text{m/s}$, 4 GHz BW

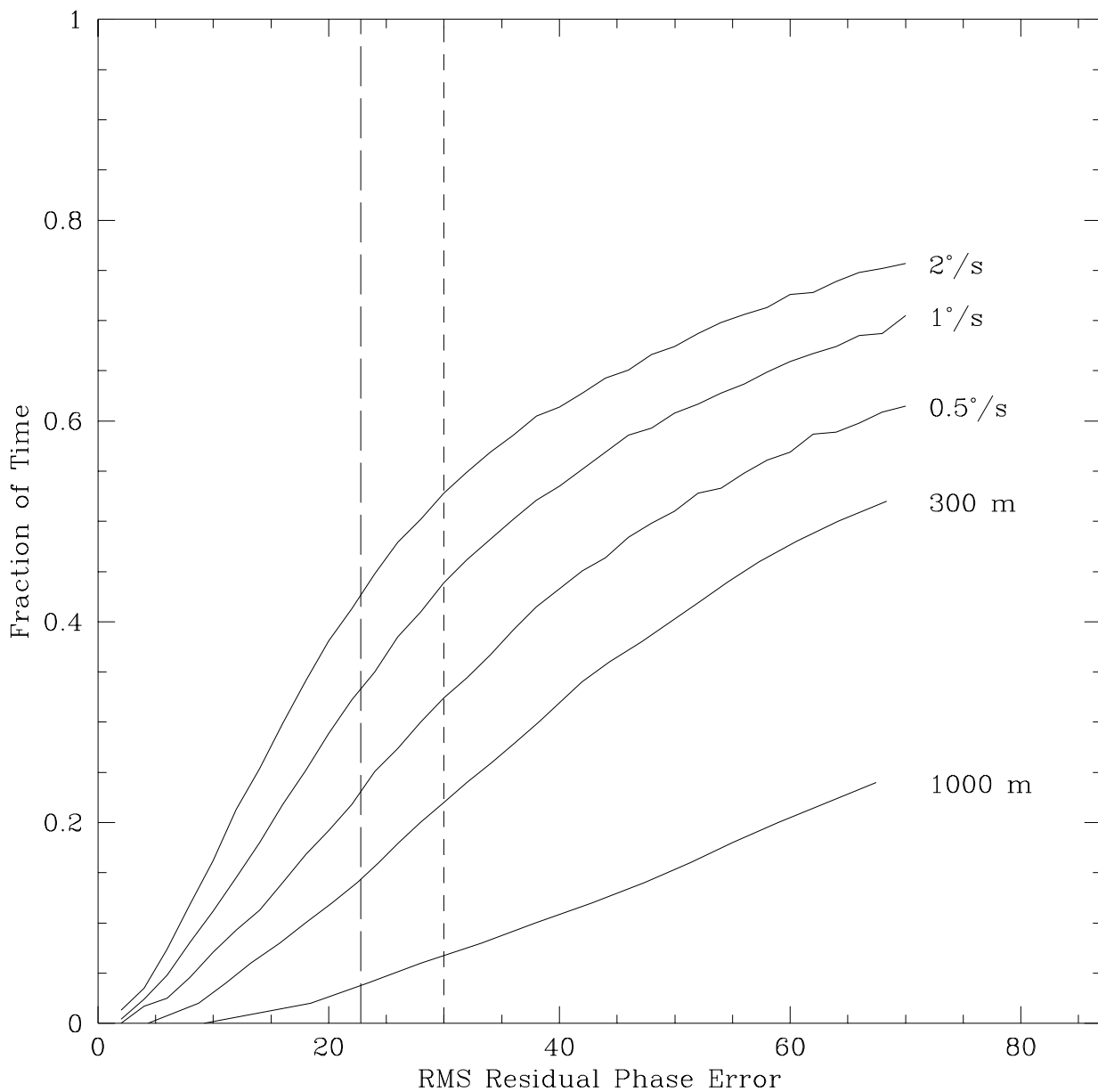


Figure 4: Cumulative distributions of residual phase errors after fast switching with 4 GHz bandwidth at the Mauna Kea VLBA site for three different switching speeds. Distributions of uncorrected atmospheric phase fluctuations on 300 m and 1000 m baselines are show for comparison.

CH and MK Residual Phase Error @ 230 GHz, $V=12\text{m/s}$, 16 GHz BW

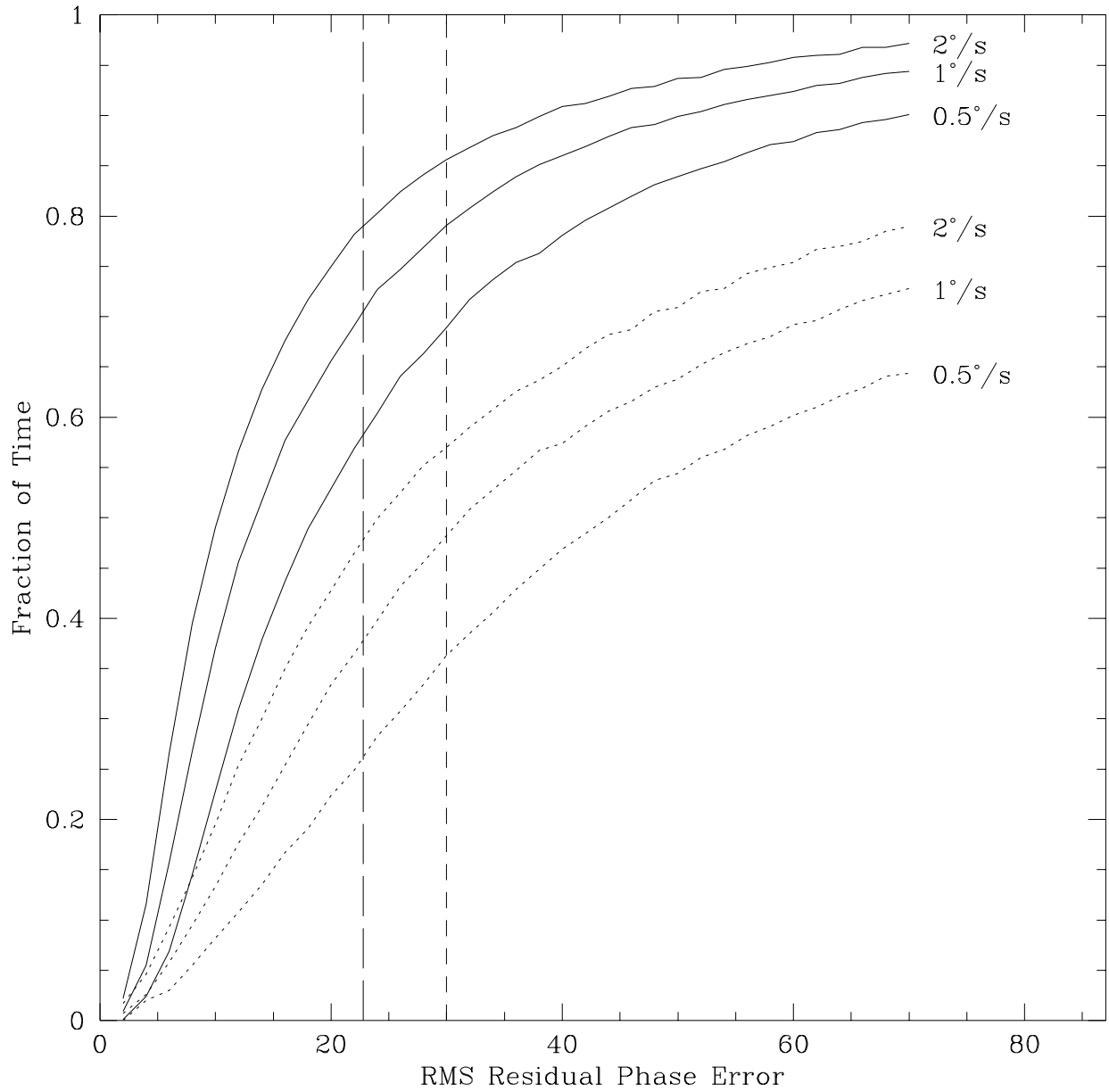


Figure 5: Comparison of cumulative distributions of residual phase errors after fast switching with 16 GHz bandwidth at Chajnantor and at Mauna Kea.

CH, 1deg/s, 230 GHz, 16 GHz BW, Different Target Source Fractions

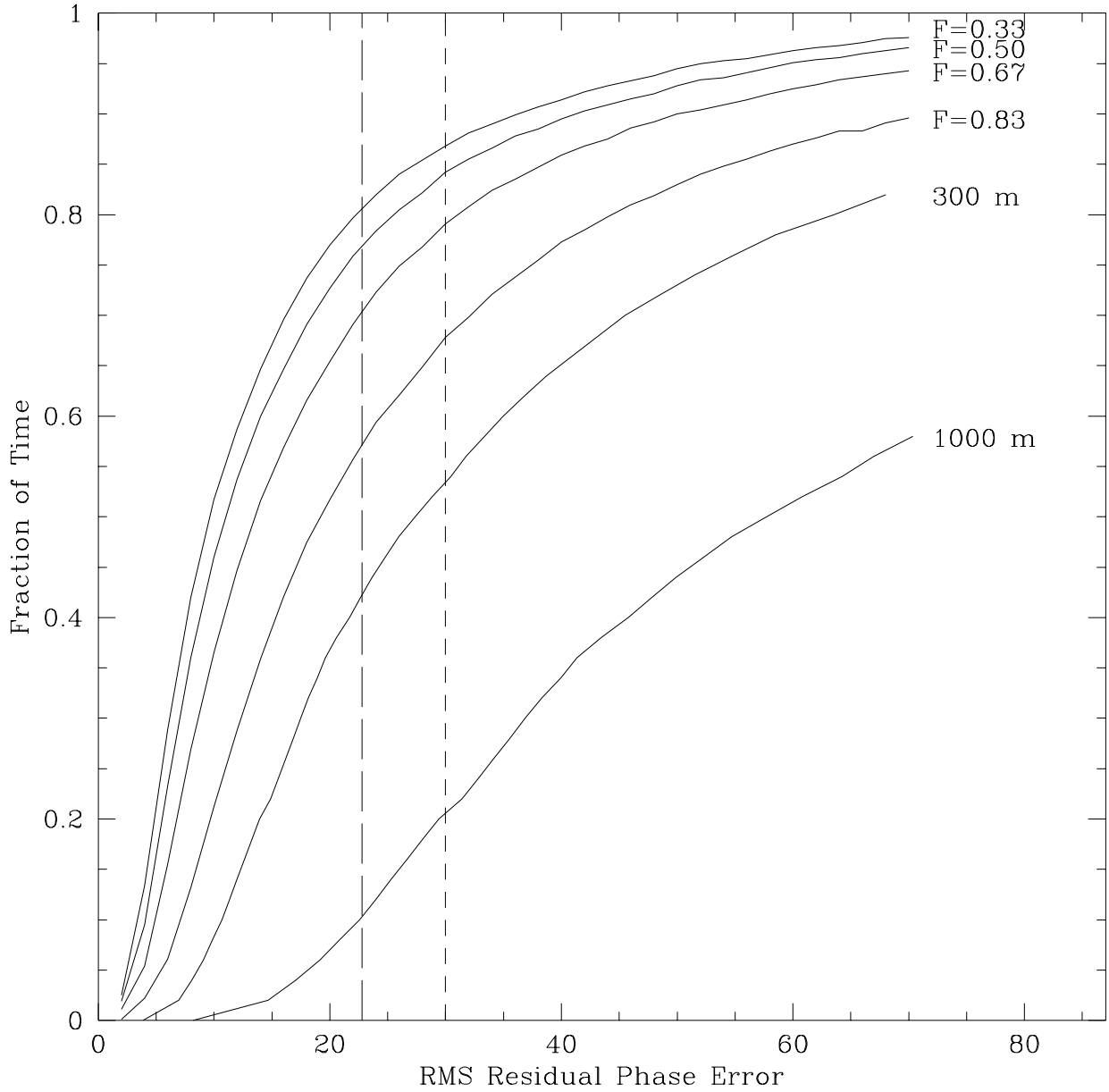


Figure 6: Cumulative distributions of residual phase errors after fast switching at 230 GHz with 16 GHz bandwidth at Chajnantor for varying fractions of time spent integrating on the target source. Since the integration time on the calibrator is fixed, smaller fractions on the target mean faster cycles. Distributions of uncorrected atmospheric phase fluctuations on 300 m and 1000 m baselines are show for comparison.